Motion of miscible magnetic fluids in a dynamic magnetic field

Ching-Yao Chen and Chi-Yuan Liao
Department of Mechanical and Automation Engineering, Da-Yeh University, Chang-Hua, Taiwan, Republic of China

Received June 2002
Revised October 2002
Accepted October 2002

Keywords *Flow, Magnetic fields, Numerical simulation*

Abstract *Displacements of a miscible magnetic layer in a capillary tube under a moving ring-shaped magnet are studied numerically. The magnet is adjusted dynamically to maintain a constant distance from the front mixing interface on the centerline. Control parameters, such as magnetic strength, effective viscosity variation due to magnetization, diffusion and the position of the magnet, are analyzed systematically. Motion of the magnetic layer is evaluated by two quantitative measurements, i.e. movement of center of gravity and spread of layer width. In general, the moving speed of the center of gravity depends only slightly on the magnetic strength, and is found slower at a higher viscosity ratio and a closer placement to the front interface as well if the magnet is placed amid the layer. A weaker spread occurs in situations of stronger magnetic strength, lower viscosity parameters and also placements near the rear interface. A multi-front finger results if the magnet is positioned ahead of the front interface.*

1. Introduction

An understanding of fluid dynamics, as well as mass transfer in a capillary tube, is important for both basic theoretical modeling and applications in the fields of hydrology, filtration and bio-engineering. Displacements subject to the conventional mechanisms, such as injection flows or gravity, have been studied thoroughly, i.e. the classical studies by Taylor (1961), Cox (1962) and corresponding calculations by Reinelt and Saffman (1985) in immiscible cases, as well as Bretherton (1961) for long bubbles. Taylor measures the amount of fluid displaced by injecting air into a horizontal capillary tube, initially filled with a viscous fluid, in order to calculate the thickness of the film of displaced fluid left behind on the wall of the tube as a function of the capillary number *Ca*. The numerical simulations by Reinelt and Saffman, based on the Stokes equations, agree very closely with these experiments. Petitjeans and Maxworthy (1996), as well as Chen and Meiburg (1996) implemented a corresponding collaborative investigation for miscible fluids. In these flows, a cutoff length is set by diffusive effects rather than surface tension, so that in some sense the Peclet number *Pe* replaces *Ca*. These authors also address finite viscosity ratios by varying the Atwood number *At*, as well as the role of

C.-Y. Chen would like to thank Professor Yamaguchi for his helpful advice on this research. The authors also express appreciation to Dr Rutledge for her editorial assistance.

International Journal of Numerical Methods for Heat & Fluid Flow
Vol. 13 No. 2, 2003
pp. 244-261

0961-5539
DOI 10.1108/09615530310459360

density differences (expressed by a further dimensionless parameter F), by conducting experiments and simulations in vertical tubes. The miscible and immiscible cases differ fundamentally in that the miscible flow can never become truly steady. Eventually, diffusion will cut off the supply of "fresh" displacing fluid, and for a long time the case of Poiseuille flow and Taylor dispersion (Taylor, 1953) will be approached.

On the other side, the development of magnetic fluids has created novel applications in similar studies with different driving forces. Magnetic fluids, which contain both flow and magnetic properties, have been widely used as devices to enhance heat transport effects due to grater thermo-magnetic free convection (Kamiyama *et al.*, 1999; Yamaguchi *et al.*, 1999a, b). In other applications, the increase in effective viscosity by the presence of magnetic field is commonly applied as a damping mechanism (Dababneh *et al.*, 1993; Raj and Moskowitz, 1980). Recently, with rapid developments in micro-devices, magnetic-force driving flows also represent potential applications in micro-scale flow fields where the traditional driving sources, such as pressure drop, are difficult to provide. In addition, mass transfer of miscible matter is crucial to improvement for better medicinal transportation, which is conventionally transported by human bio-circulation. A future application is to produce a medical solution in the form of magnetic fluid. With guidance from an external magnetic field, the medication can reach and remain at the target spot, a feat which traditional human circulation has difficulty in achieving. Chen *et al.* (2002a, b) studied the mass transfer of a miscible interface of a magnetic fluid that is transported purely by a dynamic magnetic field. They have qualitatively evaluated the effects of mass transfer under the influences of various control parameters, such as magnetic strength, viscosity variation due to the presence of a magnetic field and position of the magnet. Optional conditions of the best mass transfer factor or transferable distance were found. Here, we present the numerical simulations of a finite layer of a miscible fluid in a magnetic Stokes flow, under the influence of a moving ring-shape magnet with an additional injecting flow, to investigate the motion of magnetic fluids.

2. Governing equations

An incompressible time-dependent axisymmetric layer of a miscible magnetic fluid, having a width twice that of the tube diameter d, with front and rear mixing interfaces at $z = 9$ and 11, respectively, as shown in Figure 1, is studied. The layer is displaced by an injecting flow from the right, and subjected to the attraction of a dynamic ring-shaped magnet placed at a constant distance zm away from the front mixing interface, which is defined as the location of 0.5 average concentration across the tube section. The system of governing equations of concentration, mass and momentum is as follows:

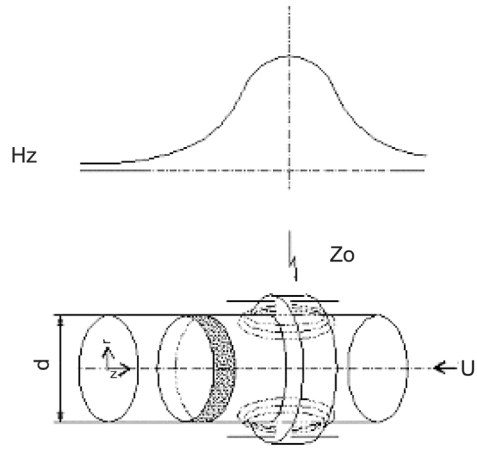

Figure 1.
Principle sketch: motion of layer of miscible magnetic fluid is driven both by injecting flow and a moving ring magnet

$$\frac{\partial c}{\partial t} + \nabla \cdot (\mathbf{v}c) = D\nabla^2 c, \tag{1}$$

$$\nabla \cdot \mathbf{v} = 0, \tag{2}$$

$$\nabla p = \nabla \cdot \tau + \mu_0 M \nabla H \tag{3}$$

where $\mathbf{v}$ is the velocity vector, and p the pressure. The stress tensor τ is defined as

$$\begin{bmatrix} \tau_{zz} & \tau_{zr} & \tau_{z\theta} \\ \tau_{rz} & \tau_{rr} & \tau_{r\theta} \\ \tau_{\theta z} & \tau_{\theta r} & \tau_{\theta\theta} \end{bmatrix} = \eta \begin{bmatrix} 2\frac{\partial v_z}{\partial z} & \frac{\partial v_x}{\partial r} + \frac{\partial v_r}{\partial z} & 0 \\ \frac{\partial v_z}{\partial r} + \frac{\partial v_r}{\partial z} & 2\frac{v_r}{r} & 0 \\ 0 & 0 & 2\frac{v_r}{r} \end{bmatrix},$$

where η is the viscosity, μ_0 represents the permeability in the vacuum, and M and H the magnetization and magnetic field, respectively. Concentration of magnetic fluid is denoted by c and the diffusion coefficient by D. It is known that the effective viscosity of a magnetic fluid increases under the presence of a magnetic field. The increase in viscosity is mainly due to the reorientation of magnetic particles when a magnetic field is applied. Various correlations of viscosity to magnetic field strength have been reported by Shliomis (1972) and Kobori and Yamaguchi (1994). Here, experimental results of a silicon oil-based magnetic fluid from Chu (1998) associated with the concentration variation are applied and take the form

$$\eta(H,c) = \eta_0 e^{a_0 Hc}, \tag{4}$$

where η_0 denotes the original fluid viscosity with zero magnetization and a_0 a material constant with a unit inverse to the magnetic strength. The magnitude of $a_0 = 0.012$ is reported by Chu (1998) for magnetic field up to 300 Oe in room temperature. The magnetization is taken in proportion to concentration c, and the M-H curve follows the Langevin function $L(\alpha_0)$ with saturated magnetization M_g,

$$L(\alpha_0) = \left(\coth(\alpha_0) - \frac{1}{\alpha_0}\right) \tag{5}$$

$$M(H,c) = M_g L(\alpha_0) c \tag{6}$$

Here, α_0 is the ratio of magnetic and kinetic energy and takes the form

$$\alpha_0 = \frac{mH}{KT}, \tag{7}$$

where m is the magnetic moment, T the temperature and K denoted the Boltzmann constant. The value of m/KT varies with the fluid properties and the local temperature. A typical magnitude of $m/KT \approx 50$ is observed by Chu (1998) under room temperature. For more details of the Langevin function, the reader can refer to Rosensweig (1985). The expression of the magnetic field is taken as the similar forms of experimental measurements in Kamiyama *et al.* (1999) and Yamaguchi *et al.* (1999a, b) as

$$H_z = H_0 F_z, \quad F_z = e^{-(z-z_0)^2} \tag{8}$$

where H_0 and z_0 determine the strength of the magnetic field and the location of the magnet. It should be noticed that the radial component of the magnetic field is neglected. When considering the current capillary tube with a small diameter, the neglect of radial magnetic strength is justified. It is further assumed that the magnetic fluid possesses the same viscosity as the non-magnetic miscible fluid when no magnetic field is applied. Thus, the viscosity variation is caused solely by external magnetic effects.

In order to render the equations dimensionless, the tube diameter d, the velocity of the Poiseuille flow profile at the centerline U, and the fluid viscosity η_0 are taken as characteristic scales, resulting in four dimensionless parameters, such as a magnetic number Mg, Peclet number Pe, magnetization number α and a viscosity parameter R defined as

$$Mg = \frac{\mu_0 M_g H_0 d}{\eta_0 U} \tag{9}$$

$$Pe = \frac{Ud}{D} \tag{10}$$

$$\alpha = \frac{mH_0}{KT} \tag{11}$$

$$R = a_0 H_0 \tag{12}$$

The viscosity parameter R leads to the local viscosity function

$$\eta = \mathrm{e}^{(RF_z c)} \tag{13}$$

The final form of the governing equation in the streamfunction Ψ formulation is

$$\frac{\partial c}{\partial t} + \nabla\cdot(\mathbf{v}c) = \frac{1}{Pe}\nabla^2 c \tag{14}$$

$$\nabla^4\Psi = -g(r,z,R,c) - Mg\frac{r}{\eta}h(r,z,H_0,c) \tag{15}$$

where function g is the viscosity term referred to by Chen and Meiburg (1996), with the replacement of c by $F_z c$, and h the magnetic force terms.

$$g = 2\left(R\frac{\partial F_z c}{\partial r} - \frac{1}{r}\right)\frac{\partial^3\psi}{\partial r^3} + 2R\frac{\partial F_z c}{\partial z}\frac{\partial^3\psi}{\partial z^3} - 2\left(\frac{1}{r} - R\frac{\partial F_z c}{\partial r}\right)\frac{\partial^3\psi}{\partial z^2\partial r} + 2R\frac{\partial F_z c}{\partial z}\frac{\partial^3\psi}{\partial r^2\partial z}$$

$$+\left\{R\frac{\partial^2 F_z c}{\partial r^3} + R^2\left(\frac{\partial F_z c}{\partial r}\right)^2 - R\frac{\partial^2 F_z c}{\partial z^2} - R^2\left(\frac{\partial F_z c}{\partial z}\right)^2 - R\frac{3}{r}\frac{\partial F_z c}{\partial r} + \frac{3}{r^2}\right\}\frac{\partial^2\psi}{\partial r^2}$$

$$+\left\{R\frac{\partial^2 F_z c}{\partial z^2} + R^2\left(\frac{\partial F_z c}{\partial z}\right)^2 - R\frac{\partial^2 F_z c}{\partial r^2} - R^2\left(\frac{\partial F_z c}{\partial r}\right)^2 - R\frac{1}{r}\frac{\partial F_z c}{\partial r}\right\}\frac{\partial^2\psi}{\partial z^2}$$

$$+2\left\{2\left(R\frac{\partial^2 F_z c}{\partial r\partial z} + R^2\frac{\partial F_z c}{\partial r}\frac{\partial F_z c}{\partial z}\right) - R\frac{1}{r}\frac{\partial F_z c}{\partial z}\right\}\frac{\partial^2\psi}{\partial r\partial z}$$

$$+\left\{R\frac{3}{r^2}\frac{\partial F_z c}{\partial r} - \frac{1}{r}\left[R\frac{\partial^2 F_z c}{\partial r^2} + R^2\left(\frac{\partial F_z c}{\partial r}\right)^2\right] + \frac{1}{r}\left[R\frac{\partial^2 F_z c}{\partial z^2} + R^2\left(\frac{\partial F_z c}{\partial z}\right)^2\right]\right.$$

$$\left. - \frac{3}{r^3}\right\}\frac{\partial\psi}{\partial r} - \frac{2}{r}\left\{R\frac{\partial^2 F_z c}{\partial r\partial z} + R^2\frac{\partial F_z c}{\partial r}\frac{\partial F_z c}{\partial z}\right\}\frac{\partial\psi}{\partial z}$$

$$h = L(\alpha F_z)\frac{\partial F_z}{\partial z}\frac{\partial c}{\partial r}$$

Boundary conditions are prescribed as

$$z = z_1, z_2 : \frac{\partial^2 c}{\partial z^2} = 0, \quad \frac{\partial^2 \psi}{\partial z^2} = 0, \quad \frac{\partial^4 \psi}{\partial z^4} = 0, \tag{16}$$

$$r = 0 : \frac{\partial c}{\partial r} = 0, \quad \psi = 0, \quad \frac{\partial \psi}{\partial r} = 0, \tag{17}$$

$$r = 0.5 : \frac{\partial c}{\partial r} = 0, \quad \psi = \frac{1}{16}, \quad \frac{\partial \psi}{\partial r} = 0. \tag{18}$$

At time $t = 0$, one-dimensional concentration fields in the form of an error function are specified on both mixing interface. The streamfunction equation is solved by the means of second-order central finite differencing discretization associated with the SLOR method and multi-grid technique. The concentration equation, which is discretized by means of four-point, third-order upwing stencils for the convective terms, and five-point, fourth-order central stencils for the diffusive terms, is solved by an ADI scheme. A constant time step $\Delta t = 0.001$ and grid size $\Delta r = \Delta z = 1/128$ are applied in the simulations. This scheme is well tested and more detailed numerical implementations can be obtained in Chen and Meiburg (1996).

3. Results

We begin by describing the temporal and spatial evolution of a reference case, in order to identify the dominant mechanisms at work. Subsequently, the values of the governing parameters, such as magnetic number *Mg*, Peclet number *Pe*, viscosity parameter *R*, magnetization number α and dynamic placement of magnet *zm* will be varied individually to elucidate their effects.

3.1 Reference cases

We first present the reference simulation of $Pe = 1,600$, $Mg = 1,000$, $R = 0$ and $\alpha = 50$, which is near the saturation point of the Langevin function. The dynamic magnet position is initially placed on the rear mixing front, i.e. $zm = 2$, and moves with the displacement of the front interface. Figure 2 displays the time sequences of the concentration field. In the present situation, the magnetic fluid is displaced towards the left by the forced convective flow, and is attracted to the right by the magnetic field. On the centerline, the convection transporting the magnetic fluid forward can be clearly identified. However, the overall convective transportation is not quite significant because of the attraction by the magnet. The movement of the major bulk of the magnetic fluid is slow. This slow movement of the magnetic fluid along the centerline allows more time for diffusion in the radial direction to proceed,

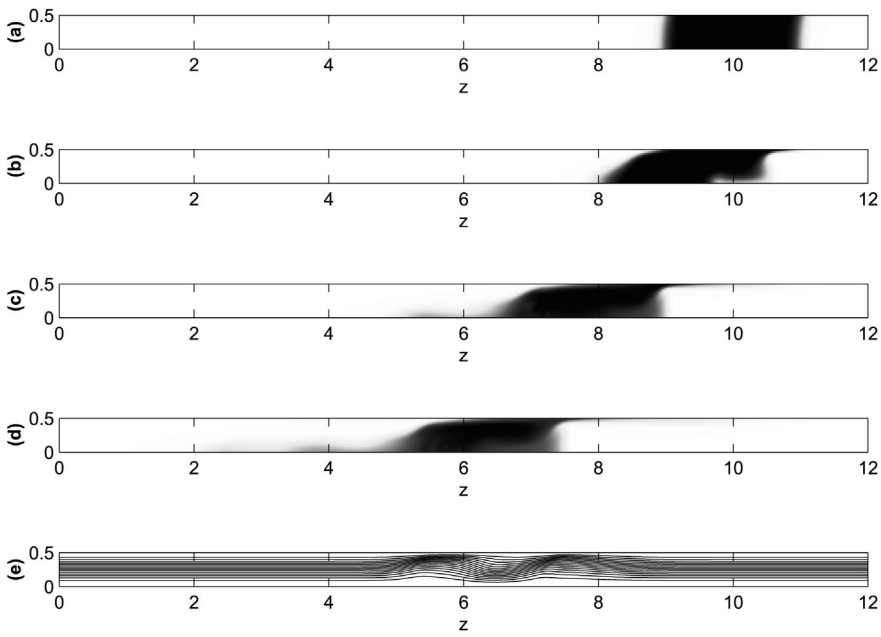

Figure 2.
Reference case: $Mg=1{,}000$, $Pe=1{,}600$, $R=0$, $\alpha=50$ and $zm=2$. Concentration fields at (a) $t=0$, (b) $t=1$, (c) $t=4$, (d) $t=7$, and (e) streamlines at $t=7$. Mixing interfaces are flat due to attraction of magnetic field placed behind. Clear detour of flow is observed near mixing interfaces

wherein mixing interfaces appear flat, even with the initial Poiseuille flow in the parabolic profile. The flat interfaces indicate a more even velocity distribution across the tube section, the velocity near the wall being accelerated with the reduction in the centerline velocity. The change in the velocity profile can be understood by the corresponding streamlines, shown in Figure 2(e). At the locations of the mixing interfaces, the detoured streamlines towards the wall are clearly shown, when compared to the parallel streamlines of the Poiseuille flow elsewhere. Another point which should be noticed is that the rear interface is much flatter than the front one. It can be attributed to the non-uniform distribution of the magnetic field. Since the current placement of the magnet is near the rear interface, this interface subjects a much stronger attraction than the front, thus leading to a flatter interface.

In order to measure the movement of the magnetic layer, the center of gravity in a magnetic fluid can be calculated as

$$C_g = 8\int_0^{12}\int_0^{\frac{1}{2}} rzc(r,z)\,\mathrm{d}r\,\mathrm{d}z, \tag{19}$$

as plotted in Figure 3. It is interesting to notice that the center of gravity is seen to move in a linear behavior with a constant rate of about -0.5, which is the average velocity of a pipe flow, despite the presence of the magnetic effect. However, the center of gravity gives only partial information concerning the

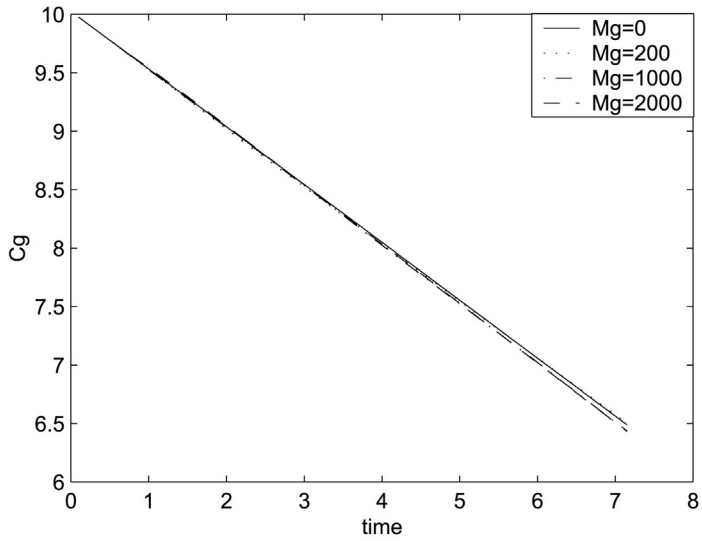

Figure 3.
Movement of center of gravity C_g at $Pe = 1{,}600$, $R = 0$, $\alpha = 50$, and $zm = 2$. Moving speed of center of gravity depends very weakly on strength of magnetic field

transportation of the magnetic layer. Another quantitative measure which should be considered is the spread in the layer. The profiles of the average concentration across tube section c_a at different times are plotted in Figure 4(a) and (b). The block of high concentration is not merely transported, but is slightly stretched as well, with a near symmetry to the center of gravity. In order to evaluate the spread of the magnetic fluid, the length of the stretched block l_{en} is defined as the distance between $c_a = 0.1$, the growth of l_{en} being displayed in Figure 5. The very insignificant growth of l_{en} reflects that the distribution of the magnetic fluid is mainly concentrated in the center of gravity without a strong spread. The weak spread in the average concentration also confirms the flat interfaces in the concentration images.

3.2 Effects of control parameters

We first discuss the influence of the magnetic number Mg, which expresses the dimensionless strength of magnetic field. An important point which should be noticed is that for certain fluid combinations and environment, in which the diffusion D, material coefficients a_0 and kinetic energy factor m/KT are fixed, the magnetic number Mg, viscosity parameter R and magnetization number α all vary with the strength of the magnetic field H_0. This fact couples the three parameters; hence they should not be treated separately. As discussed in Chen *et al.* (2002a, b), a critical strength that gives the most significant magnetic effects can be found. This critical value depends on the fluid properties, such as fluid viscosity with zero magnetization and material coefficient a_0. In order to describe the general physical behavior, Mg, R and α are analyzed separately in the present study. Displayed in Figure 6 are the concentration images

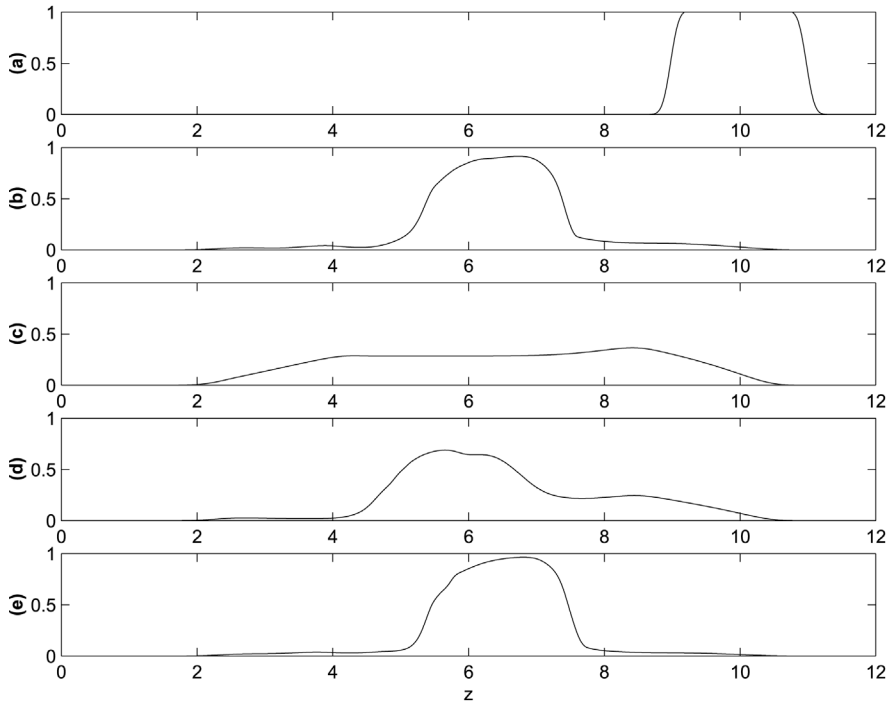

Figure 4.
Profiles of average concentration c_a for various magnetic numbers Mg at $Pe = 1{,}600$, $R = 0$, $\alpha = 50$ and $zm = 2$ for (a) initial condition, (b) $Mg = 1{,}000$ at $t = 7$, (c) $Mg = 0$ at $t = 7$, (d) $Mg = 200$ at $t = 7$, and (e) $Mg = 2{,}000$ at $t = 7$. Magnetic attraction shortens width of the layer of magnetic fluid significantly

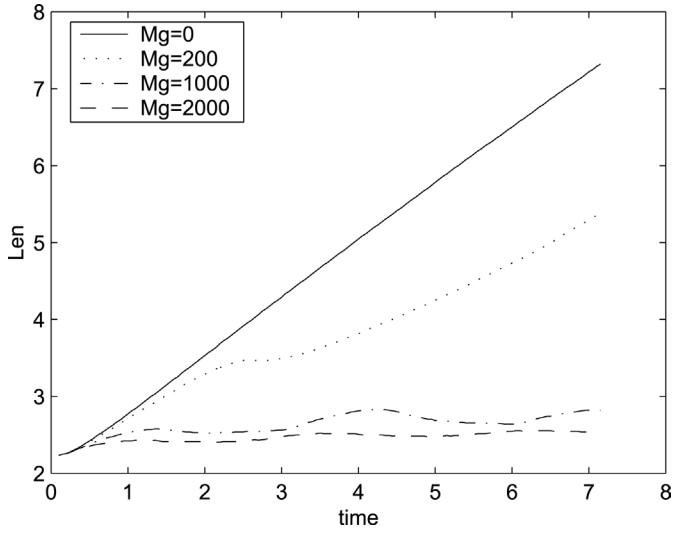

Figure 5.
Length of the layer of magnetic fluid at $Pe = 1{,}600$, $R = 0$, $\alpha = 50$ and $zm = 2$. Layer width remains almost unchanged for stronger magnetic strength $Mg = 2{,}000$, contrasted to nearly linear growth at zero magnetic field

simultaneously for various Mg with other parameters kept identical to the reference case. At zero Mg, shown in Figure 6, the flow is purely Poiseuille; thus, the mixing interfaces appear parabolic, in contrast to the flat profiles found in the reference case. Due to lack of magnetic attraction, the amount of bulk concentration is transported in a much greater quantity to the left by the strong forced convection. The increase in Mg, cf. Figure 6, clearly results in a slower moving block of magnetic fluid as well as the smaller curvatures in the mixing interfaces. In addition, the stronger magnetic field also reduces the magnetic fluid left behind near the wall region, or film thickness referred in Taylor (1961). While a significant amount of magnetic fluid still wets the wall due to the weak field locally for a zero magnetic number, very little concentration of magnetic fluid is left for Mg as high as 2,000. The fact reflects the asymmetric longtailed profile of the average concentration for the lower $Mg = 200$ in Figure 4(d) and the steeper transition of the average concentration profile at the higher $Mg = 2,000$ in Figure 4(e). The movement of center of gravity C_g shows no dependence on the magnetic field with a speed of -0.5, as displayed in Figure 3. However, the spread in concentration varies strongly in the fields, as shown in Figure 5. At zero magnetic strength, the width of the concentration layer is due to the stretch in the Poiseuille flow, for which its centerline speed is normalized to unity, and diffusion. The growth in the stretch shows a nearly constant rate that is slightly lower than 1. As the field is increased, the spread in the magnetic fluid is reduced significantly. At $Mg = 2,000$, the length of the magnetic layer remains near the initial width without a

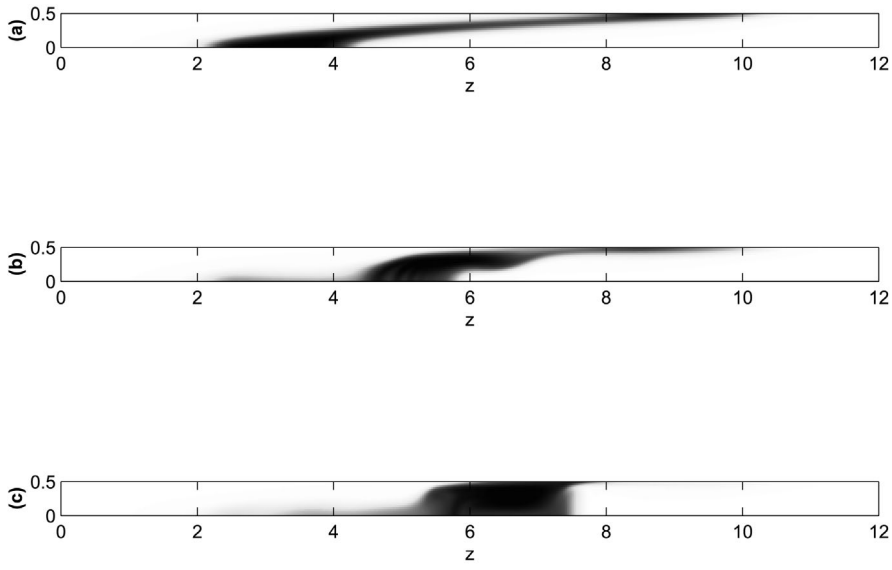

Figure 6.
Concentration fields for various magnetic numbers Mg at $Pe = 1,600$, $R = 0$, $\alpha = 50$, $zm = 2$ and $t = 7$. (a) $Mg = 0$, (b) $Mg = 200$, and (c) $Mg = 2,000$. Flatter mixing interfaces are found at higher magnetic numbers

significant spread. The nearly identical position of the center of gravity associated with a weaker spread indicates a smaller mass transport for a stronger magnetic field.

Influences of viscosity parameter R are also investigated. For a certain magnetic fluid, R is proportional to the external field, as defined in equation (10). The concentration image at $R = 2.5$, which indicates about twelve times more viscous magnetic fluid than in the environment due to magnetization, is shown in Figure 7(a) with identical Mg, Pe, α and magnet placement with regard to the reference case. Apparent influences are observed if the viscosity variance is taken into account. A flat real mixing interface is no longer preserved. Penetration of a less viscous non-magnetic fluid is also found inside the layer along the centerline. On the other hand, a blunter interface, compared to the reference case, is formed on the front side. A larger amount of magnetic fluid is left on the wall region, or referred as film. These changes can be understood by the effects of viscous stabilities. On the rear interface, a less viscous fluid displaces a more viscous one, so that the well-known Taylor-Saffman instability is perturbed. The facts of stronger fingering penetration as well as the larger film thickness left behind (Chen and Meiburg, 1996; Petitjeans and Maxworthy, 1996) agree well with the current findings. A different scenario occurs on the front interface, where the viscosity ratio is favorable. A blunter interface results from the stable viscous effect. The movement of the center of gravity and the growth in the length of the layer are displayed in Figure 8. Unlike the very weak effects of the strength of the magnetic field, the movement of the center of gravity shows a distinguishable difference at

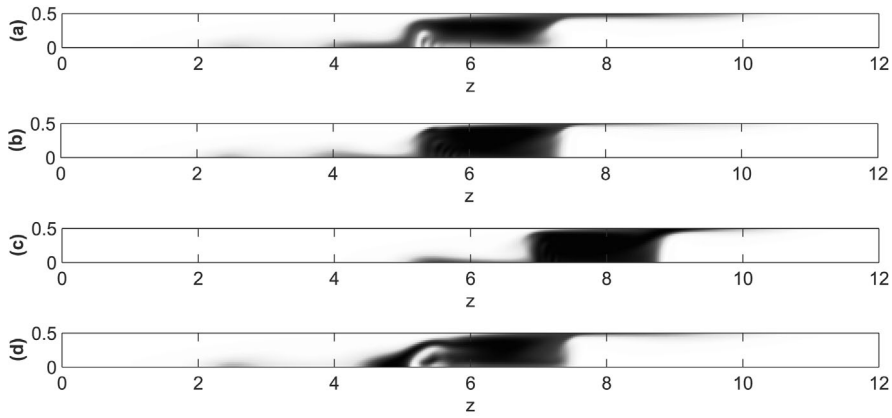

Figure 7.
Concentration fields for various control parameters $Mg = 1{,}000$ and $zm = 2$

Note: (a) $Pe = 1{,}600$, $R = 2.5$, and $\alpha = 50$ at $t = 7$, **(b)** $Pe = 3{,}000$, $R = 0$, and $\alpha = 50$ at $t = 7$, **(c)** $Pe = 1{,}600$, $R = 0$, and $\alpha = 10$ at $t = 4$ and **(d)** $Pe = 1{,}600$, $R = 0$ and $\alpha = 10$ at $t = 7$. Higher viscosity contrast leads to penetration of non-magnetic fluid on rear interface. Influences of Pe is seen insignificant. Empty area inside finger results from sudden retreat of placement of magnet due to faster decay of magnetic force

various viscosity parameters, as in Figure 8(a). Slower movement is found at a higher viscosity effect, which reflects less mobility of the magnetic fluid; thus, more is left behind to wet the wall. The spread of the layer is stronger at a higher viscosity ratio, which is also caused by the larger amount left near the wall as shown in Figure 8(b). The influences of Pe, which represents the magnitude of diffusion, are simulated as well. Shown in Figure 7(b) is the concentration image at a higher value of $Pe = 3,000$. No interesting differences are found except a weaker diffusion at the front interface, which leads to a steeper concentration gradient. In general, the influences of Pe are quite slight.

The influences of magnetization number are demonstrated by lower $\alpha = 10$ at $t = 4$ and 7, concentration fields shown in Figure 7(c) and (d), respectively. Unlike the reference case that the magnetization, governed by the Langevin function in equation (5), is nearly saturated, the current smaller magnetization number leads to a nearly linear relation between the local magnetic strength

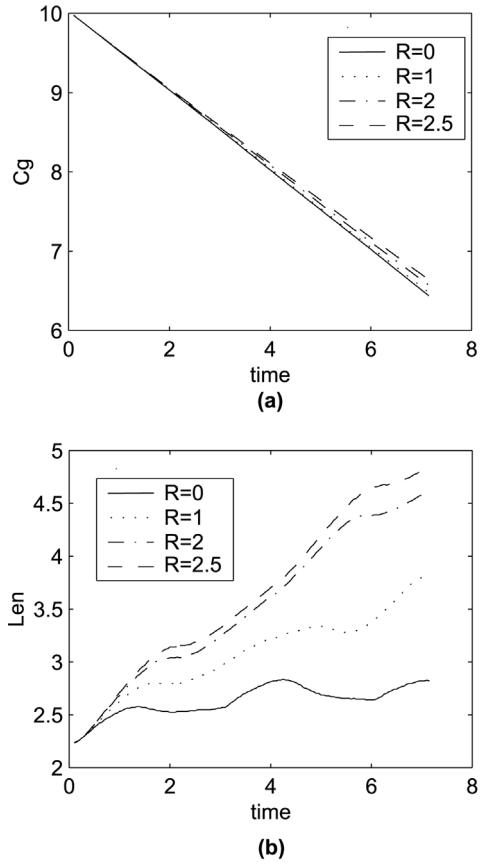

Figure 8.
(a) Movement of center of gravity, (b) length of stretched magnetic fluid layer at $Mg = 1,000$, $Pe = 1,600$, $\alpha = 50$, and $zm = 2$ for various viscosity parameters. Slightly faster movement of center of gravity and less spread are observed at lower viscosity contrast

and magnetization. A weaker and faster decay of magnetic force from the position of magnet is resulted. An apparent needle-like front interface at earlier time $t = 4$ is observed due to the fast decay of the magnetic force. This sharp needle front is unable to sustain the radial diffusion, and disperses off soon after. A sudden retreat of the front interface, defined as the location of 0.5 average concentration, is caused by the dispersion. The active control of the position of the magnet, which is adjusted to maintain a constant distance zm to the front interface, leads to a replacement of the magnet back from $z_0 = 7$ to 9. As a result, an unusual empty area inside the finger is observed at $t = 7$. It should to be addressed that even the current concentration image appears similar to the high viscosity parameter situation as shown in Figure 7(a), the mechanisms at work are quite different. For magnetization numbers higher than the reference case, no significant differences are observed due to the saturated states of magnetization. Movements of the center of gravity and spreads of the layer are shown in Figure 8 for various magnetization numbers. No significant effects are found at the center of gravity, as shown in Figure 9(a). The stretches of the layer are seen more pronounced at lower magnetization numbers due to weaker magnetic forces, displayed in Figure 9(b). The invariance of layer width for magnetization numbers greater than 50 also reflects the saturated states of magnetization.

We now focus on the effects of the position of the magnet. Several different dynamic placements zm, that is, the constant distance away from the front interface, are simulated, for which the images of the concentration are shown in Figure 10(a)-(c). Since the magnetic field decays exponentially with the distance, the placement of the magnet is expected to have major effects on the motion of the magnetic fluid, as mentioned in Chen *et al.* (2002a, b). Figure 10(a) displays the concentration image for the dynamic magnet placement right on the front interface, i.e. $zm = 0$. A very different concentration distribution from the reference case results. A faster moving and well-shaped finger with a blunt front, which resembles the patterns in the conventional displacement processes (Chen and Meiburg, 1996, 2002; Petitjeans and Maxworthy, 1996), is formed with a parabolic rear interface. The dramatic change in the concentration distribution is caused by the opposite attraction of the magnetic field. The magnetic force attracts the magnetic fluid towards the magnet, thereby orienting in opposite directions on the two sides of the magnet. While the bulk magnetic fluid is subjected to an attraction backward for $zm = 2$, the magnetic fluid is pulled forward at the current situation of $zm = 0$. As a result, a larger amount of magnetic fluid near the front interface, which is closer to the magnet and therefore subject to a greater magnetic pulling force, is transported forward in a faster path. The interface is blunter than in the case of zero magnetic force as well, due to the larger amount of transported fluid. On the other hand, a parabolic profile is preserved on the rear interface because of a weaker pulling force. Also, an interesting multi-front interface is observed

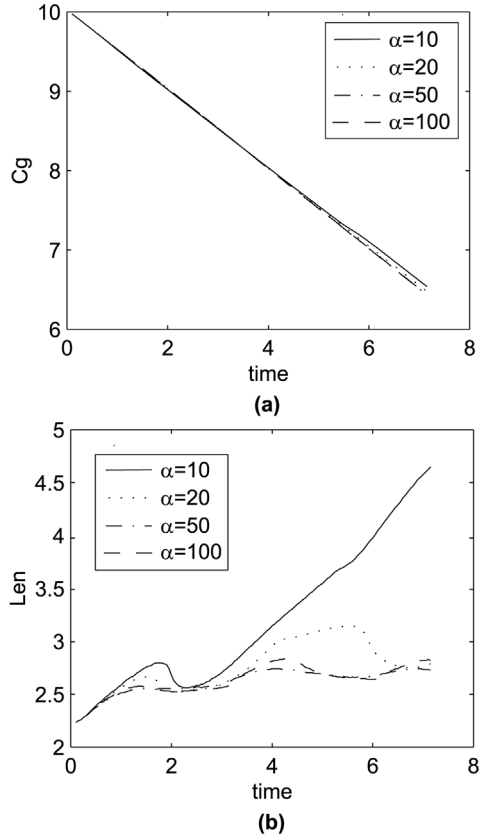

Figure 9.
(a) Movement of center of gravity, (b) length of stretched magnetic fluid layer at $Mg = 1{,}000$, $R = 0$, $Pe = 1{,}600$, and $zm = 2$ for various magnetization numbers. Movement of center of gravity depends very weakly on the magnetization numbers. Less spread is observed at higher magnetization numbers

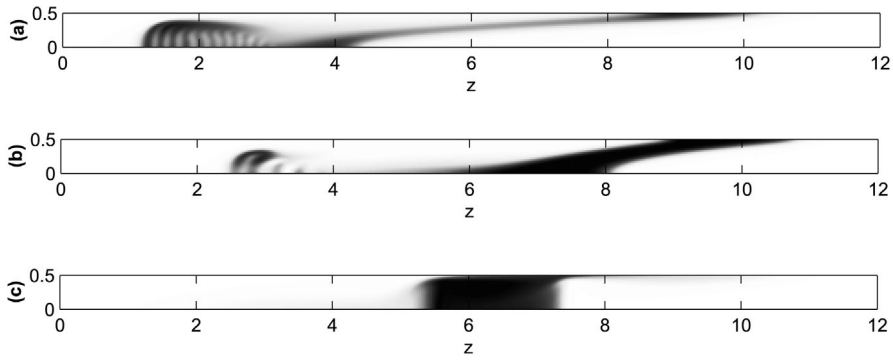

Figure 10.
Concentration fields for various placement of magnet at $Mg = 1{,}000$, $Pe = 1{,}600$, $R = 0$, and $\alpha = 50$. (a) $zm = 0$ at $t = 7$, (b) $zm = -0.5$ at $t = 4$ and (c) $zm = 1$ at $t = 7$. Placement of magnet ahead of front interface results in the formation of a fast-moving multi-front finger

inside the front finger. When considering that the magnitude of the magnetic pulling force is represented by the gradient of the field strength, as shown in momentum equation (3), zero magnetic force is generated at the location of the magnet. The dynamic position of the magnet always produces the greatest pulling force slightly behind the moving interface, thereby accelerating the fluid locally. The consequent pulling effects at a different location lead to the formation of a multi-front finger. A similar multi-front finger can also be seen for $zm = -0.5$, as in Figure 10(b). However, due to the lengthy distance to the front interface, the enhancement of the forward mass transport of the magnetic fluid by a magnetic effect is not as significant as at $zm = 0$. The front finger eventually separates the bulk magnetic fluid, in which the flow performs similarly to the situation of zero magnetic strength, as shown in Figure 6(a). If the magnet is placed amid the magnetic layer, i.e. $zm = 1$, as shown in Figure 10(c), the front interface is attracted backward while a pulling force is applied to the rear interface with the same order of magnitude, leading to a balanced distributed concentration image in which both interfaces appear evenly flat.

The influences of the position of the magnet on the movement of the center of gravity and the spread of layer length are depicted in Figure 11(a) and (b), respectively. The moving speed of the center of gravity decreases as zm is decreased, with a sudden jump at $zm = 0$. On the other hand, the length of magnetic layer tends to widen for a smaller zm. The different trends in the movement of the center of gravity and layer width can be attributed to the distinct dominance of the interfaces. When considering the displacement of zero magnetic strength, the concentration shown in Figure 6(a), a very condensed concentration is found at the front region along the centerline. In order to resist mass movement, the magnet should be placed near the front interface to preserve the concentration. This explains the slower movement of the center of gravity at a lower zm. However, once the position of the magnet is ahead of the front interface, the magnetic force reorients and pulls the magnetic fluid forward. A sudden jump in the moving speed results. In addition, Figure 6(a) also shows a long tail on the concentration left behind near the wall. The tail increases the spread length significantly even though the actual amount is not large, thus suggesting that the width of the layer is mainly affected by the real interface. Placing the magnet closer to the rear interface, therefore, significantly reduces the length of the layer. Nevertheless, the preceding argument is simply a general trend. The determination of a layer's length is also affected by the magnetic contraction at both the interfaces. The least spread is found at $zm = 1$, instead of the largest $zm = 2$, thereby indicating the maximum effect of magnetic contraction and rear interface dominance among the cases presented here.

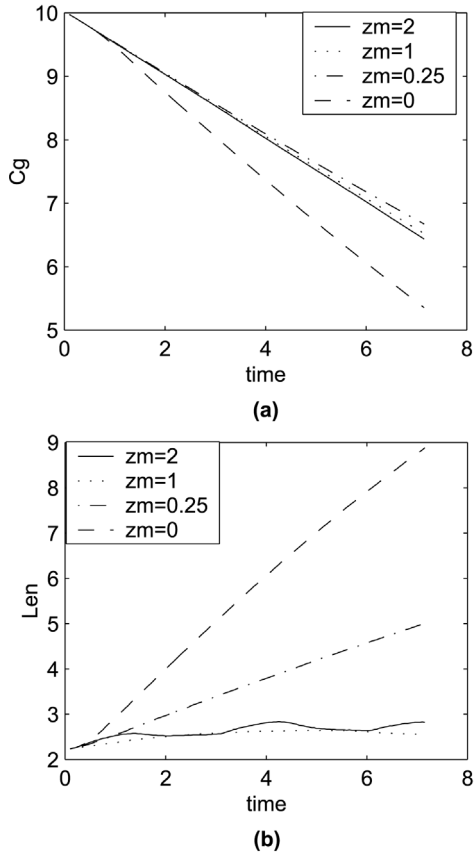

Figure 11.
(a) Movement of center of gravity, (b) length of stretched magnetic fluid layer at $Mg = 1{,}000$, $Pe = 1{,}600$, $\alpha = 50$, and $R = 0$ for various placements of magnet. Center of gravity moves slower if magnet is placed closer to and behind the front interface. A magnet placed near the rear interface in general leads to less spread

4. Conclusion

We have investigated the motion of a layer of miscible magnetic fluid in a capillary tube under a dynamic magnetic field induced by a ring-shaped magnet. The magnet has been adjusted dynamically to maintain a constant distance from the front interface on the centerline. Control parameters, such as magnetic pulling force expressed by a dimensionless magnetic number Mg, effective viscosity variation due to magnetization in a form of viscosity parameter R, diffusive effect Pe, state of magnetization α and the position of the magnet, have been analyzed systematically in order to understand their influences. If the magnet is placed behind the front interface, transportation of the bulk magnetic fluid is less significant, and the mixing interface appears flatter. The transportation of a magnetic layer has been evaluated by two quantitative measurements, the movement of the center of gravity C_g, and the length of the layer spread. In general, the moving speed of the center of gravity depends only slightly on these parameters but more on the placement of magnet. A smaller spread of magnetic fluid also results form the higher

magnetic strength because of a stronger magnetic attraction. Less mobility at larger viscosity parameters leads to a slightly slower movement in the center of gravity. The unfavorable viscosity on the rear interface, which triggers Saffman-Taylor instability, leaves more magnetic fluid behind near the wall, thus widening the magnetic layer. The influences of the position of the magnet have been observed to be more complex. In general, placement near the front interface, where massive fluids are located, leads to slow movement in the center of gravity. On the other hand, placement close to the rear interface reduces the concentration tail on the wall, and shortens the layer width. Placements of the magnet ahead of the front interface accelerate the movement of the magnetic fluid. A well-shaped, multi-front finger, similar to the conventional displacement, has been found. The influences of diffusion have been found insignificantly in the current study.

References

Bretherton, F.B. (1961), "The motion of long bubbles in tubes", *J. Fluid Mech.*, Vol. 10, p. 166.

Chen, C.-Y. and Meiburg, E. (1996), "Miscible displacements in capillary tubes. Part 2: numerical simulations", *J. Fluid Mech.*, Vol. 326, p. 57.

Chen, C.-Y. and Meiburg, E. (2002), "Miscible displacements in capillary tubes in the presence of Korteweg stresses and divergence effects", *Phys. Fluids*, Vol. 14 No. 7, p. 2052.

Chen, C.-Y., Hong, C. and Wang, S. (2002a), "Magnetic flow in a tube with the effects of viscosity variation", *J. Magn. Magn. Mater.*, Vol. 252C, p. 253.

Chen, C.-Y., Hong, C.-Y. and Chang, L. (2002b), "Mass transfer of miscible magnetic fluids in a capillary tube", *Fluid Dynamics Research* (in preparation).

Cau, I.-G. (1998), "Research of vibration control by silicon-based ferrofluid", Masters Thesis, Da-Yeh University.

Cox, B.G. (1962), "On driving a viscous fluid out of a tube", *J. Fluid Mech.*, Vol. 14, p. 81.

Dababneh, M., Ayoub, N., Odeh, I. and Laham, N. (1993), "Viscosity, resistivity and surface tension measurement of Fe_3O_4 ferrofluid", *J. Magn. Magn. Mater.*, Vol. 125, pp. 34-8.

Kamiyama, S., Ueno, K. and Yokota, Y. (1999), "Numerical analysis of unsteady gas-liquid two-phase flow of magnetic fluid", *J. Magn. Magn. Mater.*, Vol. 201, pp. 271-5.

Kobori, I. and Yamaguchi, H. (1994), "Viscosity of suspension of HTSC particles", *J. Phys. Soc. Jpn.*, Vol. 63, pp. 2691-9.

Petitjeans, P. and Maxworthy, T. (1996), "Miscible displacements in capillary tubes. Part 1: experiments", *J. Fluid Mech.*, Vol. 326, pp. 37-56.

Raj, K. and Moskowitz, R. (1980), "A review of damping applications of ferrofluids", *IEEE Transaction on Magnetics*, Vol. Mag-16.

Reinelt, D.A. and Saffman, P.G. (1985), "The penetration of a finger into a viscous fluid in a channel and tube", *SIAM J. Sci. Statist. Comput.*, Vol. 6, p. 542.

Rosenweig, R. (1985), *Ferrohydrodynamics*, Cambridge University Press.

Shiomis, M. (1972), "Effective viscosity of magnetic suspensions", *Soviet. Phys. JETP*, Vol. 34, p. 1291.

Taylor, G.I. (1953), "Dispersion of soluble matter in solvent flowing slowly through a tube", *Proc. Roy. Soc. A*, Vol. 219, p. 186.

Taylor, G.I. (1961), "Deposition of a viscous fluid on the wall of a tube", *J. Fluid Mech.*, Vol. 10, p. 161.

Yamaguchi, H., Kobori, I. and Kobayashi, N. (1999a), "Numerical study of flow state for a magnetic fluid heat transport device", *J. Magn. Magn. Mater.*, Vol. 201, pp. 260-3.

Yamaguchi, H., Kobori, I. and Uehata, Y. (1999b), "Heat transfer in natural convection of magnetic fluids", *J. Therm. Heat Transfer*, Vol. 13 No. 4, pp. 501-7.

Further reading

Chen, C.-Y., Meiburg, E. and Wang, L. (2001), "The dynamics of miscible interfaces and the effects of Korteweg stresses", *Trans. Aero. Astro. Soc. R.O.C.*, Vol. 33 No. 1, pp. 7-15.